

Bluetooth Direction Finding using Recurrent Neural Network

Pedram Babakhani
u-blox Berlin GmbH
Berlin, Germany
pedram.babakhani@u-blox.com

Ioannis Sarris
u-blox Athens S.A
Athens, Greece
ioannis.sarris@u-blox.com

Timon Merk
u-blox Berlin GmbH
Berlin, Germany
timon.merk@u-blox.com

Dimitris Kalogiros
u-blox Athens S.A
Athens, Greece
dimitris.kalogiros@u-blox.com

Matthias Mahlig
u-blox Berlin GmbH
Berlin, Germany
matthias.mahlig@u-blox.com

Peter Karlsson
u-blox Malmö AB
Malmö, Sweden
peter.karlsson@u-blox.com

Abstract— Multipath propagation in an indoor environment has a detrimental impact on the performance of Angle of Arrival (AoA) estimation methods due to the existence of obstacles introducing reflections and scattering. This paper proposes a new architecture for AoA estimation, utilizing a robust and fast signal processing algorithm and a small Recurrent Neural Network (RNN) to improve performance by considering AoA estimation as a time series problem. The proposed method uses the Spatial Power Spectrum (SPS) of the well-established Propagator Direct Data Acquisition (PDDA) algorithm as an input feature for a Gated Recurrent Unit (GRU), which enhances the accuracy of PDDA by learning dependencies of spatial power spectrum features through previous time steps. Experimental results on a simulated rectangular indoor environment, with four different obstacle sets, show significant performance benefits (PDDA MAE = 7.0° vs GRU MAE = 3.7°) of GRU. Furthermore, the proposed method outperforms PDDA in a real indoor environment measurement (PDDA MAE = 12.2° vs GRU MAE = 7.1°). Additionally, the proposed method is sufficiently small in size (830 kB) to be employed on a wide range of embedded systems.

Keywords—Angle of Arrival, Recurrent Neural Network, Gated Recurrent Unit, Indoor Positioning, Direction Finding, Deep Learning

I INTRODUCTION

Indoor positioning and Direction Finding (DF) became a challenging research topic over the last few decades due to the high demand in industrial and IoT applications. Bluetooth direction-finding methods are based on determining the Angle of Arrival (AoA) of received signals between a mobile Bluetooth tag and an antenna array. Classic AoA estimation techniques commonly involve spectral-based methods as ESPRIT [1] and Multiple Signal Classification (MUSIC) [2], based on IQ sample covariance matrix calculation, which is computationally complex and might not be feasible in real-time applications, where high resolution and quick responses are required. Subsequently, Propagator Direct Data Acquisition (PDDA) [3] was proposed as an efficient, fast, and robust spatial AoA estimation method with low complexity. PDDA avoids covariance matrix construction, eigenvalue decomposition, and matrix inverse computation. Furthermore, PDDA needs no prior knowledge about the number of signal sources despite the MUSIC and the ESPRIT methods [3].

Recently, Machine Learning (ML) and Deep Learning (DL) techniques have gained high attention due to their capabilities to learn hidden structures in input data. An early DL-based method called Radial Basis Function Neural Networks (RBFNN) (El Zooghby, 1997) [4] has shown the potential of DL in AoA estimation.

Afterward, a multi-layer perceptron (MLP) model using the spatial covariance matrix as a feature set (Agatonović et al. 2013) [5] outperformed the MUSIC method on real measurements. Additionally, a Deep Neural Network (DNN) using raw IQ values (Bialer et al. 2019) [6] has demonstrated the strength of DNN in AoA estimation. Furthermore, Gaussian Process (GP) and Regression Tree (RT) based methods using the Spatial Power Spectrum (SPS) of MUSIC (Khan et al. 2018) [7][22] have gained outstanding performance in Azimuth and Elevation estimation. Additionally, SPS has been exploited as input features of Recurrent Neural Network (RNN) in positioning [8], which has achieved remarkable performance due to its ability to identify long and short-term dependencies of sequential data. Long Short Term Memory (LSTM) [9] and Gated Recurrent Unit (GRU) [10] are well-known RNN architectures and are widely used for time-series predictions. Recently, several RNN based methods have been proposed for indoor positioning and direction-finding [11][12].

The effectiveness of time series prediction in indoor positioning has been investigated by applying LSTM on Received Signal Strength (RSS) sequences (Sahar et al. 2018) [13]. Similarly, GRU has achieved considerable performance in indoor positioning by learning time dependencies of RSSI values in sequential paths [14]. Furthermore, GRU has shown strong potential in dynamic navigation [15].

We assume that non-linear time dependencies of SPS are effective in direction finding while the tag used for tracking the AoA is shifting frequently from Line of Sight (LOS) to Non-Line of Sight (NLOS) in an indoor environment. We consider direction finding as a time series forecasting problem where the current direction is derived based on previous time step directions. We propose a robust and efficient RNN-based method (tinyDL) [16] for AoA estimation. The proposed architecture utilizes PDDA as a robust preprocessing algorithm that extracts input features (Spatial Power Spectrum) for a GRU that captures dependencies through time and updates its contents dynamically. We show that Spatial Power Spectra from different transmission frequency channels can be used as an input feature and how NLOS affects the SPS of different Bluetooth frequency channels. Furthermore, we compare the performance of the RNN based method with multiplied PDDA (elementwise multiplied of multi-SPS) in a simulated and real environment with different specifications and set of obstacles. Our investigations show that the proposed method outperforms multiplied PDDA in all different simulated and real hardware measurement scenarios, irrespectively of the used antenna specification.

II RECURRENT NEURAL NETWORK

RNN architectures are applied to a wide range of applications such as translation [17], sequence learning [18], and time series forecasting [19]. The most well-known RNN models are Long Short Term Memory (LSTM) and Gated Recurrent Unit (GRU) models. In real-time direction finding applications, DL models should be fast and small in size to be deployed on embedded systems. Therefore, GRU has advantages compared to LSTM due to less computational complexity, which makes GRU an RNN model feasible for real-time embedded platforms [20]. Indoor direction finding can be considered as a time series problem that can be solved by utilizing RNN models. Generally in RNN models, the output of each time step is derived based on the input of the current time step and the output of the previous time steps. Fig 1. shows the structure of RNN for T time steps where X, H, and O represent input, recurrent, and output units consecutively.

As depicted in Fig. 1, our proposed method input is the multi-SPS acquired from three Bluetooth channels, and the output is the estimated AoA at each time step t using a recurrent unit model referred to as GRU.

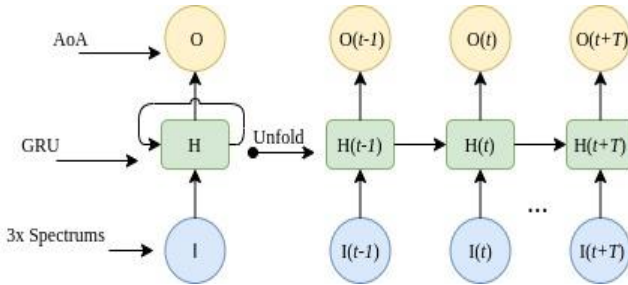


Fig. 1: Recurrent Neural Network in AoA estimation

The sequential and nonlinear dependency of predictions at each time step on the previous step is assumed to be effective in AoA estimation. Assume a tag is frequently moving from a LOS to an NLOS area in an indoor environment, therefore considering the previous time steps can mitigate AoA estimation error.

II.A. Gated Recurrent Unit

GRU is a self-adaptive recurrent neural unit that is able to capture dependencies at various time steps adaptively and updates itself accordingly [10]. GRU consists of three feed-forward neural networks (FFNNs) units and two gates called reset and update gates.

Reset gate: GRU decides to consider the calculated hidden output of the previous time step or ignore it and consider the input as a start of a new sequence.

Update gate: GRU decides how much of its content should be updated according to the previous time step.

Subsequently, GRU computes the nominated output for the current time step. Eventually, the final output of the current time step is computed based on the output of the update gate, the output of the previous time step. Fig. 2 displays two gates and three computational units based on input and previously computed hidden output. Reset and update gates are indicated as r_t and z_t respectively.

X_t , \hat{h}_{t-1} , and h_t represent input, nominated output, and final output correspondingly. Tanh and Sigmoid are activation functions.

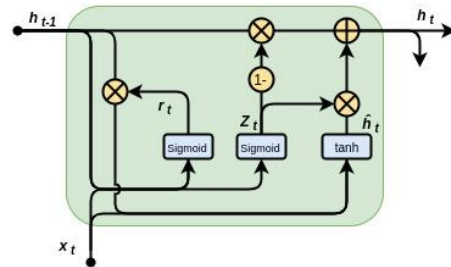


Fig. 2: GRU block diagram

III METHODOLOGY

Generally, incident signals are analog sinusoidal signals frequently transmitted between a sender and receiving antenna with no prior information about whether the signal is transmitted directly or propagated through multiple component propagation within an indoor environment. Analog signals are demodulated into IQ values using two sinusoids with the same frequency and a relative phase shift of 90°. We acquire raw IQ values through three Bluetooth advertising channels: channels 37, 38, and 39 at 2.402, 2.426, and 2.480 GHz respectively. Afterward, the PDDA algorithm is applied as a feature extractor on the raw IQ values acquired from every channel separately. PDDA constructs SPS density based on IQ values and the corresponding angle to the most powerful received signal is the PDDA AoA estimation. PDDA predicts AoA based on the corresponding angle to the peak of the SPS.

We concatenate SPS of three channels horizontally. Assume that $P(t)$ is the horizontal concatenation of three SPSs, obtained through three channels at time step t as the following:

$$P(t) = [P_{CH37}(\phi_t), P_{CH38}(\phi_t), P_{CH39}(\phi_t)] \quad (1)$$

$P(t)$ corresponds to the raw feature and $P(\phi_t)$ represents the SPS of a single channel at time step t . Eventually, $P(t)$ is standardized as the following:

$$F(t) = \frac{P(t) - \mu}{\sigma} \quad (2)$$

Where μ and σ are the mean and standard deviation of the feature vector $P(t)$. Finally, a series of standardized features obtained through previous time steps (snapshots) is fed into a GRU to predict AoA based on previous predictions and features. The length of every time step is predefined manually by the antenna specification and sampling rate. The number of considered previous time steps in GRU can vary arbitrarily. The main idea behind using GRU for AoA estimation is to capture time dependencies of previous time steps (e.g 1-7 steps for a walking agent) adaptively. GRU can ignore erroneous predictions and consider reasonable estimations of previous steps and update the recurrent unit content accordingly at each time step. This idea can improve AoA estimation in the transition between LOS to NLOS and vice versa by remembering and learning the dependencies of the previous steps. Fig. 3 depicts the diagram of the proposed architecture from incident analog signals to AoA estimation.

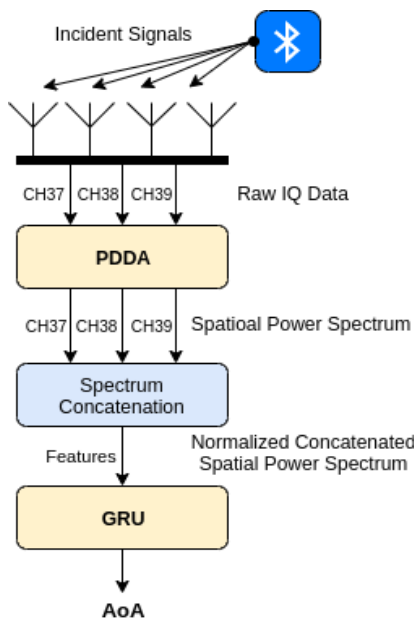


Fig. 3: Block diagram of proposed AoA estimation technique

IV DATA ACQUISITION

IV.A. Simulated Data

Simulated data provides the possibility of defining an infinite number of paths and sequences within an environment where it can create more scenarios. Consequently, DL models are trained and tested on more data points which make a model more robust. We simulated a 98 m^2 ($14\text{m} \times 7\text{m}$) rectangular environment with four different sets of obstacles shown in Fig. 4 using RayTracing simulation software (Radio Coverage Planning with Altair WinProp)[23]. The simulated environment is equipped with four isotropic Bluetooth 5.1 anchors installed on each corner of the ceiling. The transmission power of each anchor is specified as +4 dBm.

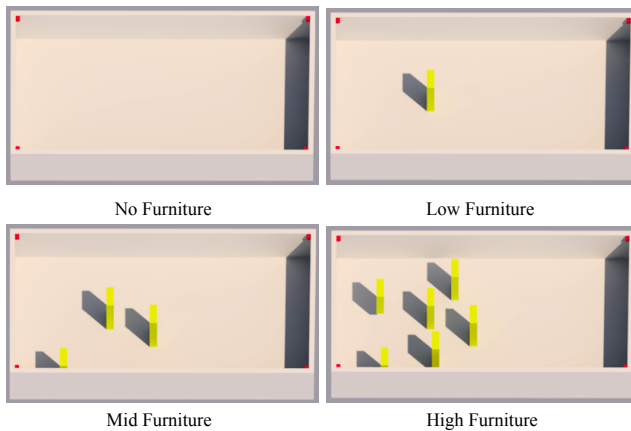


Fig. 4: 3D view of the simulated indoor environments. Pillars are shown in yellow and anchors are displayed in red cubes.

The simulated environment covers 2450 coordinates with a grid of 20 cm intervals between adjacent simulation sampling points. According to each anchor, we sampled 2450 snapshots per channel separately, therefore every anchor in each environment includes 7350 snapshots totally. Consequently, each environment comprises 29400 measurements.

IV.B. Real Hardware Measurement

In addition to the evaluated simulation data, we further tested the proposed deep learning method for AoA prediction on real hardware measurements in a real indoor environment. Approximately 15000 snapshots through three channels of a linear L-shape Bluetooth antenna array have been recorded from a transmitting tag moving in a real indoor environment (70 m^2) including reflective materials through pillars, obstacles and furniture. Fig. 5 shows the floor plan of the real environment. The ground truth or real angle labels for each data point have been measured using 4 Ultra-Wideband (UWB) anchors shown as blue dots. Additionally, there is a concrete pillar in front of the antenna displayed in gray, introducing a strong NLOS area, making direction-finding more challenging.

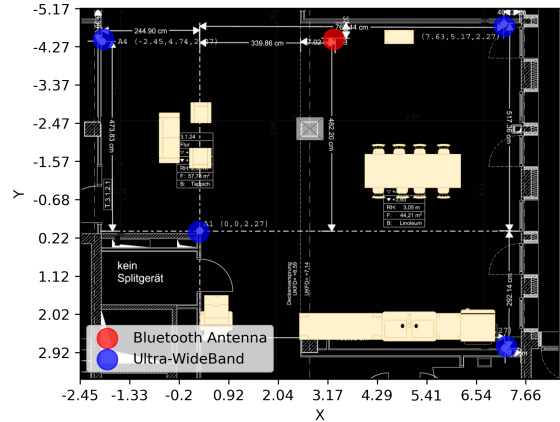


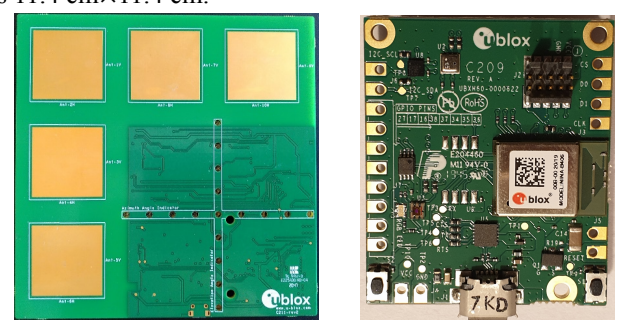
Fig. 5: Real hardware measurement indoor floor plan, providing a typical multipath propagation environment.

Fig. 6 shows the stationary antenna and the real indoor environment consisting of windows, obstacles and furniture.



Fig. 6 Real indoor environment consisting of obstacles, furniture, and reflective surfaces.

Fig. 7 shows the antenna array and the Bluetooth 5.1 transmitting tag used for the real hardware measurements. The antenna array consists of two planes where the x-axis and y-axis calculate the phase shift of azimuth and elevation respectively. In this study, we focus on 2D direction finding and azimuth prediction therefore only antenna elements along the x-axis have been used. The reference antenna element is located on the corner. Furthermore, the transmission power is +4dBm. The antenna board dimension is $11.4 \text{ cm} \times 11.4 \text{ cm}$.

L-shape Bluetooth Antenna Array Bluetooth tag
Fig. 7: Real hardware measurements platforms

IV.C. Deep Learning Features

The PDDA is applied to the IQ values of received signals through every channel separately. Eventually, there is an SPS vector of size $1 \times N$ acquired from every channel. Hypothesize that the measurement resolution is 1 degree therefore the size of the spatial power spectrum for each channel is 1×181 including spatial power value for every angle in the range of $\{-90^\circ, -89^\circ, \dots, 0^\circ, \dots, 89^\circ, 90^\circ\}$. The PDDA reference estimation for AoA is the corresponding angle to the maximum spatial power value in the spectrum. Fig. 8 displays the SPS for the simulation environment for every channel and the true angle according to the four simulated environments equipped with four anchors. Additionally, the standard deviation across each spectrum is shown shaded. The standard deviation is calculated across all sample coordinate points that are aligned with the true depicted angle.

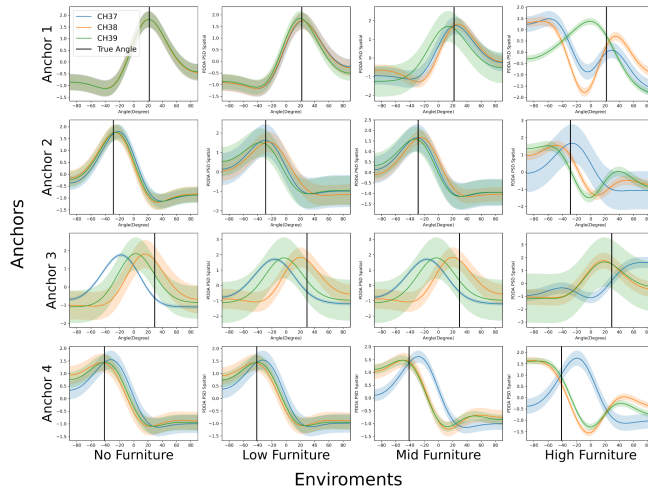


Fig. 8: Environment, anchor, and channel-specific features. PDDA Spatial power spectrum densities vary with transmission frequency (channel) for all used anchors and respective environments.

The global maximum of every spectrum is chosen as PDDA AoA estimation according to every channel. Fig. 8. shows that generally the SPS is affected by each channel, anchor, and environment. Furthermore, it shows the specific performance of every channel utilizing PDDA for AoA estimation. Fig. 9 shows how LOS and NLOS are affecting the SPS obtained from three channels for different environments. As visible, spectrums can be uncorrelated in the NLOS area but show more correlation in the LOS measurements, causing different AoA estimations across channels for the NLOS case. This shows that PDDA can be highly affected by NLOS settings, while a deep learning architecture can learn the channel-specific dependencies for a specific environment for high-performance AoA prediction.

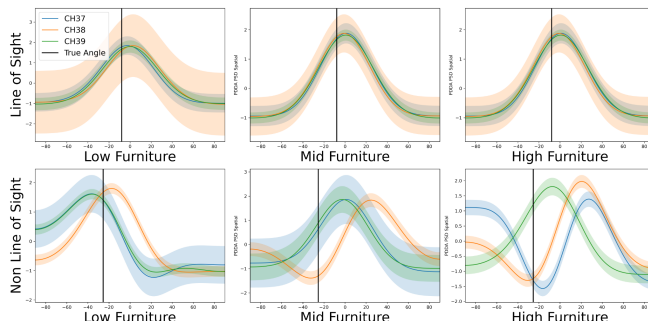


Fig. 9: Non Line of Sight specific features. NLoS impacts PDDA spatial power spectrum features throughout different channels and environments

V EXPERIMENTAL RESULTS

Experimental results are based on a GRU with 32 hidden units followed by two fully connected layers consisting of 16 neurons individually as is shown in Fig. 10. This architecture has been found through hyperparameter search.

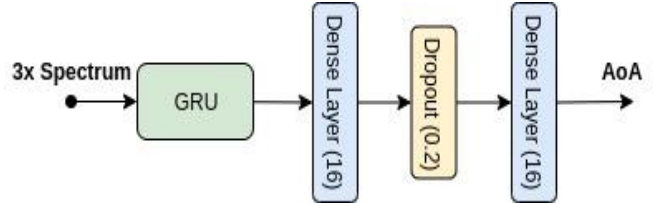


Fig. 10: Stacked GRU and dense layer architecture for AoA estimation given PDDA spatial power spectrum as input features

We have trained GRU with constant hyperparameters for all experiments using Adam optimizer[21] with a learning rate of 0.0001 and batch size of 10 for 100 epochs. Furthermore, reported results according to PDDA are derived based on element-wise multiplication of spectrums obtained from every channel, and the corresponding angle with the highest power value in the multiplied spectrum is chosen as AoA estimation of PDDA. Experimental investigations have shown that multiplied channels PDDA improves PDDA estimation compared to a single channel.

Generally, in all experiments, the last three time steps are considered for each time step prediction. This means the last three previous input features are concatenated to the current input and the current prediction is affected by previous time steps prediction. Additionally, cross-validation is a known method for model evaluation in ML and DL. Here we use a 5 fold CV for testing the performance within a specific environment and for a specific anchor. Additionally, we report experimental results on training the model in one specific environment and test the model on other environments to investigate how the model can be generalized in different environments. MAE is computed as the following:

$$\text{MAE} = \frac{1}{N} \sum_{i=0}^N |y - \hat{y}| \quad (3)$$

Here y and \hat{y} represent a true angle and predicted angle respectively. N indicates the number of tested samples. We compare the performance of multiplied PDDA and the proposed method based on MAE, relational t-test of error distributions, and cumulative distribution function (CDF) 90% confidence error. Furthermore, we compare general errors for predicted angles in bins of 2° and 3° acquired from all experimental results in the real measurements.

V.A. Simulation Data Results

We have selected paths randomly through different coordinates to make stochastic and random scenarios within the simulated environment. Each path includes a long sequence of SPS and true angles of a moving tag relative to each anchor. We have considered a distance limit in random paths where the distance of two consecutive data points cannot exceed more than 1 meter to simulate a moving tag of walking speed. On the other hand, azimuth angles are varying in the range from -45° to 45° because anchors are installed on the corners and the field of view is 90° .

All experiments have been trained by 50% of coordinates (1225 data points) and tested by 50% (1225 data points), hence the train and test paths are uncorrelated due to not sharing exact coordinates within random paths. Furthermore, training and testing the model equally on the same number of data points lead to approximately the same distribution of NLOS and LOS which can generalize the model inclusively.

Error distributions of experiments according to every anchor and environment are displayed in Fig. 11. In all different simulated environments, GRU outperforms PDDA by lower MAE and error distribution. Furthermore, the t-test is an inferential statistic for two distribution comparisons. Therefore, our investigation based on relational t-test shows significant improvement where p-values for all experiments are less than 0.1% shown in Fig. 11.

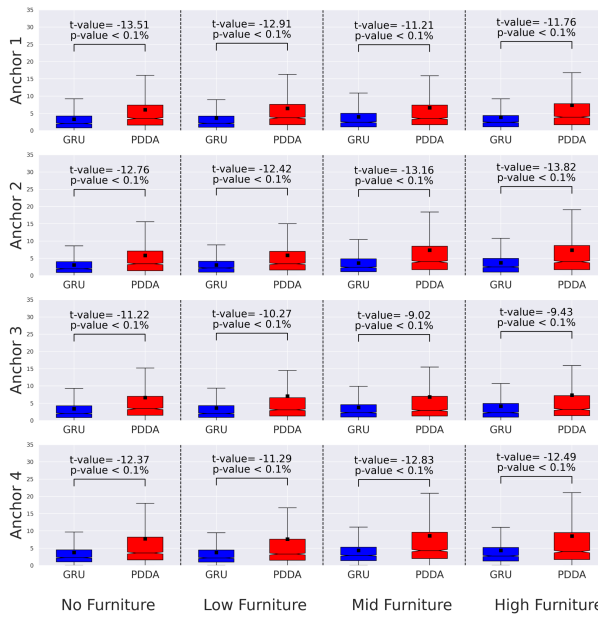


Fig. 11: AoA error comparison for different anchors and different environments between GRU and PDDA. Throughout every environment and anchor measurement, GRU outperformed PDDA significantly.

Furthermore, GRU ensures an error of less than 12° with a confidence of 90%, and it has been significantly enhanced compared to multiplied PDDA performances. Fig. 12 indicates the CDF of errors based on all experimental results according to every anchor and environment.

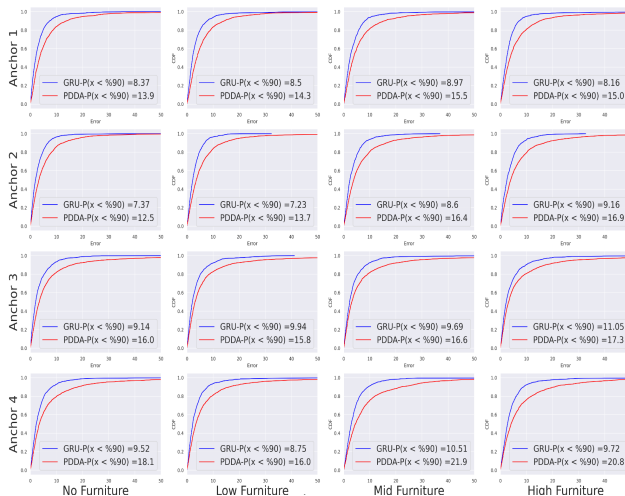


Fig. 12: PDDA and GRU CDF 90% confidence error reveals the higher performance of GRU over PDDA for every anchor and environment.

The MAEs of experimental results are reported in Table 1 separately according to each environment and anchor. Table 1 reports that in all experiments and scenarios, GRU improves MAE compared to PDDA performance.

Table 1: MAE comparison of GRU and PDDA

Anchor	No Furniture		Low Furniture		Mid Furniture		High Furniture	
	GRU	PDDA	GRU	PDDA	GRU	PDDA	GRU	PDDA
1	3.3°	6.0°	3.6°	6.4°	4.0°	6.6°	3.9°	7.0°
2	3.0°	5.8°	3.1°	5.8°	3.6°	7.3°	3.8°	7.4°
3	3.4°	6.6°	3.6°	7.0°	3.8°	6.9°	4.4°	7.8°
4	3.7°	7.7°	3.7°	7.6°	4.3°	8.6°	4.6°	8.8°

Fig. 13 compares the PDDA and GRU performances by displaying errors on the High Furniture environment floor plan according to each anchor by assuming a moving tag. As it is displayed, GRU outperforms PDDA according to all anchors especially behind obstacles introducing NLOS area.

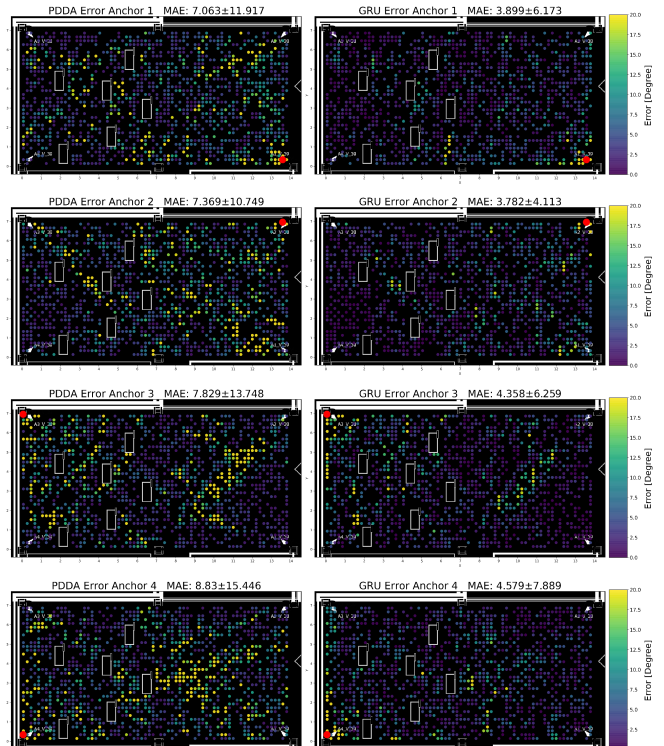


Fig. 13: GRU vs PDDA error comparison in the simulated High Furniture environment according to each anchor. Anchors are displayed as red dots. The absolute AoA error shows that GRU outperforms PDDA while PDDA has lower performance in LOS and NLOS.

To investigate further how the trained GRU model performs towards environmental changes, we trained the GRU in a specific simulated environment and cross-tested it on the other environments to show the robustness of the method towards environment changes through e.g. an added obstacle (Fig. 4). The environment cross prediction results in Fig. 14 show the MAE of each experiment based on training on a specific environment and testing on the other environments according to each anchor.

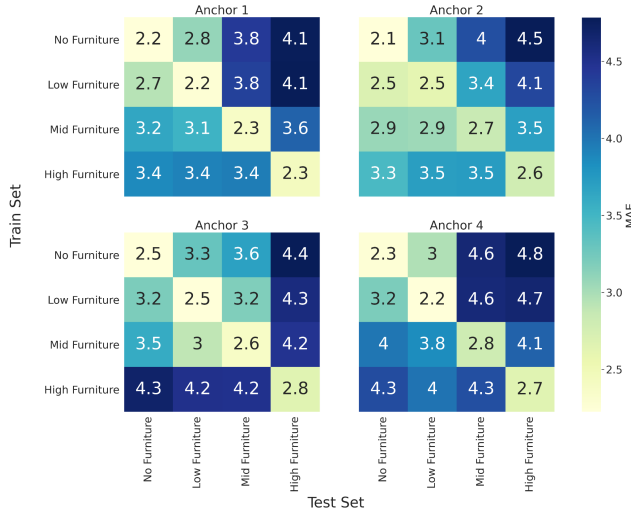


Fig. 14: Environment cross prediction MAE GRU results. Trained environments are shown on the y axis, while the testing environments are on the x-axis respectively for every anchor. GRU model performance shows here that AoA predictions can still be predicted with high accuracy towards environmental changes.

Compared to the PDDA MAE in Table 1, the GRU MAE for the altered environment predictions shows that the used deep learning method outperforms PDDA despite environmental changes. Fig. 14 proves that the proposed method can robustly generalize across different sets of unobserved obstacles and environments.

V.B. Real Hardware Measurement Results

After concatenation of three channels across 15000 snapshots, approximately 5000 data points have been acquired in the real hardware measurements. Angles are varying between -90° to 90° because the Bluetooth antenna is installed on a tripod with a height of 1.5 m and the field of view is 180° . The raw IQ values are acquired from three channels, similar to the simulated data. The model has been trained with the same hyperparameters and training rate as simulation. The proposed method outperforms here the multiplied PDDA similarly, where MAE has been improved significantly from 12.2° to 7.1° . Fig. 15 shows the error distributions and compares the error threshold with a confidence of 90% in PDDA and GRU according to the real measurements. Additionally, t-test statistics prove a significant improvement in GRU compared to the multiplied PDDA errors.

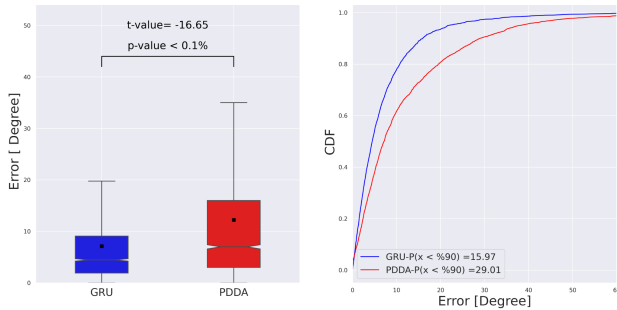


Fig. 15: (Left) Error distributions of PDDA and GRU in real hardware measurements.

(Right) PDDA and GRU CDF error and 90% confidence of error

Fig. 16 compares PDDA and GRU errors in the real measurements by visualizing the error of each time step across the floor plan of the real environment. As it is shown, GRU outperforms PDDA by considering the last three previous steps, the main difference is more visible in the NLOS area located on both sides of the antenna in an angle range of more than 45° and less than -45° , indicating edges

where signals may not be received directly from a sender and probably signals are propagated through obstacles. Additionally, GRU reveals higher accuracy behind the pillar (displayed in gray) in front of the antenna.

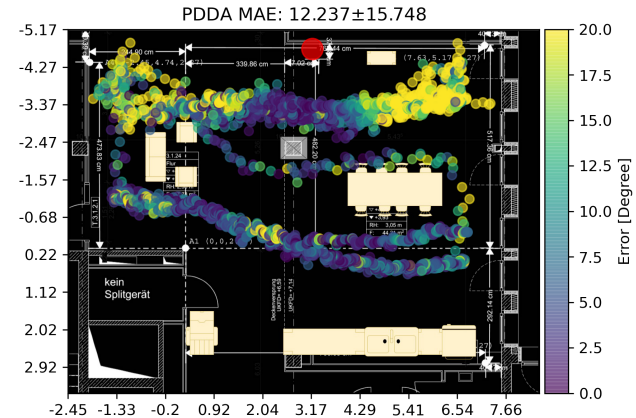
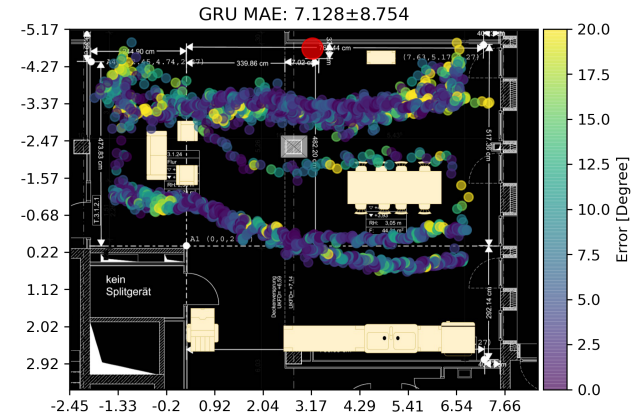


Fig 16: GRU vs PDDA error comparison in the real hardware measurements. The antenna position is displayed as the red dot. The absolute AoA error shows that GRU outperforms PDDA. While PDDA suffers from poor edge and NLoS performance, GRU model performance can be trained for such environment specifics.

Fig. 17 displays all tested data points obtained in a real environment and it compares PDDA and GRU estimation error for all predicted angles in bins of 3° . GRU outperforms PDDA, especially in NLOS areas located on both sides of the antenna. Furthermore, the NLOS (pillar) effect is visible in an angle range of -20° to -10° , where GRU indicates higher accuracy considerably.

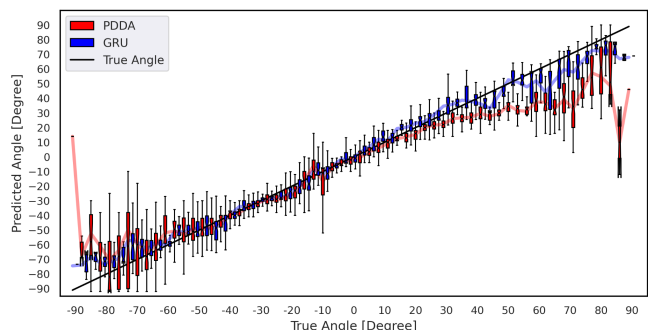


Fig 17: GRU vs PDDA predictions in the real environment

V.C. Model Size

Every deep learning model size depends on the number of parameters and floating-point precision format. The number of GRU parameters is computed as the following:

$$g \times [h(h+i) + h] \quad (4)$$

Where g is the number of FFNNs, h is the number of hidden units and i is the input dimension. The g is a constant number that equals 3.

According to the proposed method, the GRU consists of 32 hidden units. Furthermore, the input dimension equals 4 times the current input feature, because the last three steps input features are concatenated at each time step. Additionally, the number of features equals 543 (3×181), therefore the input dimension is 2172 (4×543). Fully connected layers consist of 528 and 272 parameters. The number of parameters is calculated as the following:

$$3 \times [32(32+2172) + 32] + 528 + 272$$

Consequently, the proposed model has 212480 trainable parameters. The model size is approximately calculated by multiplying the number of parameters and floating-point precision format. We assume that the precision format is float32 (4 bytes), the model size is 830 kB capable of being stored in memory (RAM, Flash) of modern embedded systems. Fig. 18 shows model size and MAE based on different considered previous steps of real measurements. As it is shown on the left side, the model size and number of considered previous steps have a linear relation according to equation (4). Additionally, MAE has been decreased by increasing the considered number of previous steps displayed on the right side. The model can be altered according to application requirements and embedded systems storage and processing capacity.

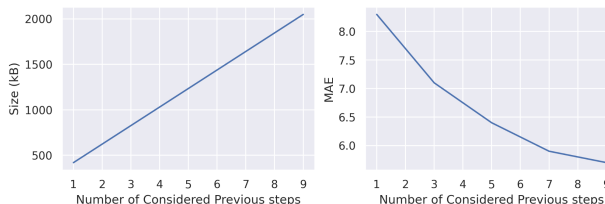


Fig 18. (Left) Number of considered previous steps vs model size
(Right) Number of considered previous time steps vs MAE

VI CONCLUSION

Generic AoA methods are highly affected by multipath component propagation in an indoor environment where obstacles cause high errors due to scattering, reflection, and fraction. Furthermore, classic AoA techniques are time-independent algorithms where previous time steps are not considered in the current prediction. Primarily, we assume AoA estimation as a time series problem where time dependencies are captured. Secondly, we utilize spatial power spectrums of PDDA as input features acquired from three Bluetooth channels to extract more features and predict AoA more precisely. In this paper, we proposed an architecture combining PDDA as a feature extractor, and GRU as an RNN model to enhance the performance of AoA by learning previous states and predictions dependencies through time. We have shown that utilizing three channels is effective especially in NLOS where SPSs of different channels are uncorrelated. Our investigations based on MAE and comparison based on t-test have shown significant improvements compared to PDDA in a simulated and real hardware environment. Furthermore, the proposed method generates less error confidently based on CDF 90% confidence error comparison. Additionally, cross-validation proves the robustness of the proposed architecture towards environmental changes based on training on specific environments and testing on the other environments. The proposed method outperforms multiplied PDDA, especially in the NLOS area, which proves the assumption of time series effectiveness. Additionally, the proposed RNN architecture is sufficiently small to be implemented on embedded systems. All in all, we showed the potential in

utilizing the RNN model for direction finding which is capable of being adjusted according to application requirements. Through the simulation data, optimal task-specific parametrization can be performed and applied in a real measurement setting.

REFERENCES

- [1] A. Paulraj, R. Roy and T. Kailath, "Estimation Of Signal Parameters Rotational Invariance Techniques- Esprit," Nineteenth Asilomar Conference on Circuits, Systems and Computers, pp. 83-89, 1985.
- [2] H. MONOSON "STATISTICAL DIGITAL SIGNAL PROCESSING AND MODELING". NEW YORK: JOHN WILEY&SONS, 1996.
- [3] M. Al-Sadoon, N. Ali, Y. Dama, A. Zuid, S. Jones, R. Abd-Alhameed, and J. Noras, "A New Low Complexity Angle of Arrival Algorithm for 1D and 2D Direction Estimation in MIMO Smart Antenna Systems," Sensors, vol. 17, Nov. 2017
- [4] A. H. El Zooghby, C. G. Christodoulou and M. Georgopoulos, "Performance of radial-basis function networks for direction of arrival estimation with antenna arrays," IEEE Trans, Antennas and Propagation, vol. 45, no. 11, pp. 1611-1617, November 1997
- [5] M. Agatovic, Z. Stankovic, I. Milovanovic, NS. Doncov, L., T. Zwick, B. Milovanovic. "Efficient Neural Network Approach for 2D DOA Estimation Based on Antenna Array Measurements," Progress In Electromagnetics Research, Vol. 137, 741-758, 2013.
- [6] O. Bialer, N. Garnett and T. Tiler, "Performance Advantages of Deep Neural Networks for Angle of Arrival Estimation," IEEE International Conference on Acoustics, Speech and Signal Processing (ICASSP), pp. 3907-3911, 2019.
- [7] A. Khan, S. Wang and Z. Zhu, "Angle-of-Arrival Estimation Using an Adaptive Machine Learning Framework," IEEE Communications Letters, vol. 23, no. 2, pp. 294-297, February 2019,
- [8] K. Sayrafian-Pour, D. Kaspar "Indoor positioning using spatial power spectrum," IEEE 16th International Symposium on Personal, Indoor and Mobile Radio Communications, vol. 4, pp. 2722-2726., April 2005.
- [9] F.A. Gers, J. Schmidhuber, F. Cummins. "Learning to forget: Continual prediction with LSTM." Ninth International Conference on Artificial Neural Networks (ICANN), pp. 850-855 vol.2, 1999.
- [10] J. Chung, C. Gulcehre, K. Cho, Y. Bengio. "Empirical evaluation of gated recurrent neural networks on sequence modeling," NIPS Workshop on Deep Learning, December 2014.
- [11] Y. Lukito, A.R. Chrismanto. "Recurrent neural networks model for WiFi-based indoor positioning system," International Conference on Smart Cities, Automation & Intelligent Computing Systems (ICON-SONICS), pp. 121-125, February 2017.
- [12] M. T. Hoang, B. Yuen, X. Dong, T. Lu, R. Westendorp and K. Reddy, "Recurrent Neural Networks for Accurate RSSI Indoor Localization," IEEE Internet of Things Journal, vol. 6, pp. 10639-10651, December 2019.
- [13] A. Sahar, D. Han. "An LSTM-based indoor positioning method using Wi-Fi signals". Second International Conference on Vision, Image and Signal Processing, pp. 1-5, August 2018.
- [14] J. Wang, C. Guo, L. Wu. "Gated Recurrent Unit with RSSIs from Heterogeneous Network for Mobile Positioning". Mobile Information Systems. 2021 Apr 13;2021.
- [15] J. Yuan, H. Wang, C. Lin, D. Liu and D. Yu, "A Novel GRU-RNN Network Model for Dynamic Path Planning of Mobile Robot," in IEEE Access, vol. 7, pp. 15140-15151, February 2019.
- [16] B. Darvish Rouhani, A. Mirhoseini and F. Koushanfar, "TinyDL: Just-in-time deep learning solution for constrained embedded systems," 2017 IEEE International Symposium on Circuits and Systems (ISCAS), pp. 1-4, 2017.
- [17] M. A. Gangi, M. Negri, M. Turchi, "Adapting transformer to end-to-end spoken language translation".International Speech Communication Association (ISCA), pp. 1133-1137. 2019.
- [18] I . Sutskever, V. Oriol, V. Le Quoc, "Sequence to sequence learning with neural networks" In Proceedings of the 27th International Conference on Neural Information Processing Systems - MIT., Vol.2 November 2014.
- [19] M. Hüskes, P. Stagge. "Recurrent neural networks for time series classification." Neurocomputing pp.223-235, 2003.
- [20] N. M. Rezk, M. Purnaprajna, T. Nordström and Z. Ul-Abdin, "Recurrent Neural Networks: An Embedded Computing Perspective," in IEEE Access, vol. 8, pp. 57967-57996, 2020,
- [21] DP. Kingma, BA. Jimmy. "Adam: A method for stochastic optimization." arXiv preprint arXiv:1412.6980 2014.
- [22] T. Merk, M. Abou Nasa, F. Rezai, P. Karlsson, M. Matthias, "Machine Learning calibration of Angle of Arrival methods based on different experimental Unified Linear and Rectified Array measurements". TechRxiv. 2021.
- [23] R. Hoppe, G. Wölfle and U. Jakobus, "Wave propagation and radio network planning software WinProp added to the electromagnetic solver package FEKO," International Applied Computational Electromagnetics Society Symposium(ACES), pp. 1-2, 2017.